Follow up month, (median) (IQR)	6 (4-8)	
Recurrence at first follow up (%)	19.5	15.8 – 23.7
Histo-pathology at first follow-up: (%)		
Tubular adenoma	68.1	56.1 – 77.2
Sessile serrated adenoma	17.4	10 – 28.4
Tubullovillous adenoma	13.0	6.8 – 23.4
Villous adenoma	1.5	0.2 – 9.9
Adenocarcinoma	0	0 – 0.9%
Second follow up, No (%)	218 (56)	
Recurrence at second follow up (%)	11.5	7.9 – 16.5
Histo-pathology at second follow-up: (%)		
Tubular adenoma	75	53.1 – 88.8
Sessile serrated adenoma	12.5	3.8 – 33.9
Tubillovillous adenoma	12.5	3.8 – 33.9
Villous adenoma	0	0 – 1.7
Adenocarcinoma	0	0 – 1.7
Third follow up, No (%)	74 (19)	
Recurrence at third follow-up (%)	6.8	2.8 – 15.4
Histo-pathology at third follow-up: (%)		
Tubular adenoma	60	10.6 – 95
Sessile serrated adenoma	20	1.1 – 84.8
Tubillovillous adenoma	20	1.1 – 84.8
Villous adenoma	0	0 – 4.9
Adenocarcinoma	0	0 – 4.9

Table 2 follow up results

Sa1651

PLASMA BASED CELL-FREE CIRCULATING TUMOR DNA (CTDNA) ASSESSMENT FOR NON-INVASIVE DETECTION OF COLORECTAL CANCER (CRC)

Jason Dean, Yupeng He, Victoria Raymond, Seung Tae Kim, Jeeyun Lee, Hee Cheol Kim, Ariel Jaimovich, AmirAli Talasaz

Background: Multimodal approaches to colorectal cancer (CRC) screening are necessary in order to increase patient compliance with guideline recommendations. Non-invasive blood-based CRC screening is a patient preferred screening method, however currently available modalities lack sufficient sensitivity and specificity for widespread adoption thus hindering utilization. We previously presented data demonstrating high sensitivity (90%) and specificity (89%) of a blood-based CRC assay (Kim, et al. CCR 2019). Here we evaluate clinical performance characteristics of the same methods on appropriately selected colonoscopy screened-negative controls. **Methods:** Blood was collected from 524 participants from three categories a) age-matched colonoscopy screened negative controls with blood collected prior to colonoscopy (N=185), b) age-matched self-declared cancer-free controls (N=196), and c) colon cancer positive cases with blood collected prior to surgical resection (N=143; 64-Stage I/II; 37-Stage III; 42-Stage IV). Participant samples were divided into testing and training sets. Total cell-free DNA (cfDNA) was extracted, partitioned based on methylation level, and analyzed using the LUNAR assay, a targeted panel optimized for genomic and epigenomic (methylation and fragmentomics) modifications associated with CRC (Guardant Health, CA). **Results:** The original machine learning model was trained on 109 samples (38 with Stage IV CRC and 71 age-matched self-declared cancer-free controls) and a threshold was determined to match a target specificity based on the training samples. When applying our original model to the colonoscopy screened negative controls, the observed specificity was higher than that observed on self-declared cancer-free controls: for 90% specificity targeted model, the test set specificity improved from 89% to 94% (see Figure 1; 111/125 self-declared cancer-free controls; 174/185 colonoscopy screened negative controls). Using new thresholds targeting 90% specificity based on a training set of 100 colonoscopy screened negative samples, the ctDNA detection rate in CRC positive cases was 92% (97/105) at 91% specificity as measured with an independent test set of 85 colonoscopy screened negative controls (89%-Stage I/II, 97%-Stage III, 100%-Stage IV) as compared to 90% sensitivity (95/105) at 89% specificity using self-reported cancer-free controls (88%-Stage I/II, 95%-Stage III, 100%-Stage IV). Similar improvements were observed for 95% and 98% specificity targeted models. **Discussion:** These results have significant implications for the clinical utility of combined genomic and epigenomic ctDNA analysis for CRC detection and suggest that some of the previous false positive samples may correspond to undiagnosed malignancies or adenomas in unscreened participants.

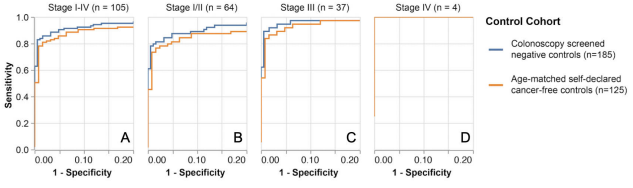

Figure 1: Receiver Operator Curves (ROC) of the machine learning model. The specificity is based on either 185 colonoscopy screened negative controls (blue line) or 125 age-matched self-declared cancer free controls (orange line- Kim et al CCR 2019). Sensitivity is based on the same cohort of 105 patients with CRC and is presented in all 105 CRC cases (A), 64 cases with Stage I/II CRC (B), 37 cases with Stage III CRC (C), and 4 cases with Stage IV CRC (D).

Sa1652

ARTIFICIAL INTELLIGENCE-AUGMENTED VISUALIZATION WITH REAL TIME HISTOLOGY MAPPING OF COLORECTAL POLYPS

Eladio Rodriguez-Diaz, Gyorgy Baffy, Wai-Kit Lo, Hiroshi Mashimo, Gitanjali Vidyarthi, Shyam S. Mohapatra, Satish K. Singh

OBJECTIVE: Artificial intelligence (AI) within computer-aided diagnostic (CADx) algorithms can enable real-time histology (RTH) of colonic polyps. We report a method that renders both border detection and accurate RTH in a pseudocolor histology map video overlay. METHODS: In an IRB-approved study, widefield and near-focus NBI polyp images were obtained during screening/surveillance exams with Olympus EVIS EXERA III CF-HQ190L colonoscopes at three tertiary care facilities. Images were correlated to index pathology. We designed a deep learning algorithm encompassing: 1. Semantic segmentation, to delineate polyp boundaries automatically, and 2. Region-of-interest (ROI) based classification (64 x 64 pixels) within a segmented polyp. ROIs within the polyp boundary were classified independently and combined to generate a pseudocolor histology map superimposed onto the polyp during endoscopy (**Figure 1**). We used 740 images from 607 polyps in 286 patients to train and validate the semantic segmentation network. Over 30,000 ROIs were used to train and validate the classification network. A distinct testing set consisting of 349 images from 205 polyps from 87 patients was used to evaluate performance. RESULTS: A mean intersection-over-union (IOU) score of 0.82 with a 96.4% detection sensitivity was obtained as part of the segmentation step of the algorithm. Subsequent classification of 195 polyps, 125 neoplastic (including serrated polyps/adenomas) and 70 non-neoplastic, resulted in an overall sensitivity (Se) of 95%, specificity (Sp) of 83%, negative predictive value (NPV) of 89% and high confidence rate (HCR) of 87%. Restricting the analysis to the 70 neoplastic and 63 non-neoplastic diminutive polyps ≤ 5mm resulted in a Se=94%, Sp=88%, NPV=92%, and HCR=85%. In 55 rectosigmoid polyps ≤ 5mm (2 neoplastic, 53 non-neoplastic) that potentially could be left behind if non-neoplastic per the ASGE PIVI guidelines, a Se=100%, Sp=91%, NPV=100%, and HCR=84% was obtained. CONCLUSION: Results from this multi-site study indicate that our automated CADx approach provides (1) delineation of polyp boundaries, (2) simultaneous pseudocolor histology maps of individual polyps, and (3) RTH performance in line with PIVI thresholds. Our CADx seeks to be less of a decision "black box" in that it displays the algorithm at work defining boundaries and making spatial histological assessments that inform the overall polyp classification. We believe that presenting augmented visual information in real time in this manner has the potential to improve operator performance and guide clinical decisions in a more intuitive, accurate, and user-friendly manner. Finally, images of polyps with histology maps may serve as a truly automated "optical biopsy" equivalent to traditional histopathology for the purposes of documentation in electronic health records.

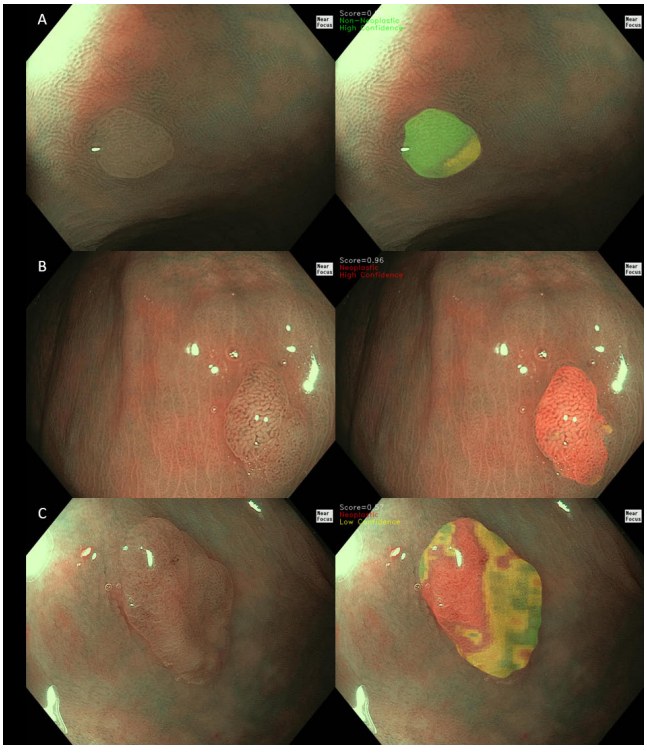

Figure 1: Typical RTH visualization of polyps by our CADx with border delineation and histology mapping: (A) hyperplastic, (B) adenomatous, and (C) serrated polyps. Red=high confidence neoplastic, Green=high confidence non-neoplastic, Yellow=indeterminate or low confidence regions.